Chinese Journal of Aeronautics 25 (2012) 372-380

Contents lists available at ScienceDirect

Chinese Journal of Aeronautics

journal homepage: www.elsevier.com/locate/cja

Visualization Experiments of a Specific Fuel Flow Through Quartz-glass Tubes Under both Sub- and Supercritical Conditions

DENG Hongwu[a], ZHANG Chunben[a,b,*], XU Guoqiang[a], TAO Zhi[a], ZHU Kun[a], WANG Yingjie[a]

[a] *National Key Laboratory of Science and Technology on Aero-Engine Aero-thermodynamics, School of Jet Propulsion, Beihang University, Beijing 100191, China*

[b] *Xi'an Aerospace Propulsion Institute, Xi'an 710100, China*

Received 5 May 2011; revised 8 June 2011; accepted 29 August 2011

Abstract

The present work is a visualization study of a typical kerosene (RP-3) flowing through vertical and horizontal quartz-glass tubes under both sub- and supercritical conditions by a high speed camera. The experiments are accomplished at temperatures of 300-730 K under pressures from 0.107-5 MPa. Six distinctive two-phase flow patterns are observed in upward flow and the critical point of RP-3 is identified as critical pressure p_c=2.33 MPa and critical temperature T_c=645.04 K and it is found that when the fluid pressure exceeds 2.33 MPa the flow can be considered as a single phase flow. The critical opalescence phenomenon of RP-3 is observed when the temperature is between 643.16 K and 648.61 K and the pressure is between 2.308 MPa and 2.366 MPa. The region filled by the critical opalescence in the upward flow is clearly larger than that in the downward flow due to the interaction between the buoyancy force and fluid inertia. Morecover, obvious layered flow phenomenon is observed in horizontal flow under supercritical pressures due to the differences of gravity and density.

Keywords: visualization; flow patterns; critical opalescence; supercritical; layered; fuel

1. Introduction

The efficient cooling technology is one of the critical methods to reduce the thermal stress and heat load of the turbine components in modern engines. Fuel-cooled aircraft thermal management systems are popularly used with the minimum weight penalty and technical risk [1]. The versatile affordable advanced turbine engines (VAATE) and integrated high performance turbine engine technology (IHPTET) program show that more and more cooling requirements are needed, and then the fuel temperature is through and beyond the critical region due to the limited fuel supply. The thermophysics properties of fuel are required to be well-known for the safety of application. The database of properties of the fuel such as vapor pressure, specific heat, density, viscosity, surface tension and critical parameters is necessary to predict the performance of components and to shorten the design cycle of engine. Systematic studies of those thermophysics properties of mixtures and their excess properties can give insight into the molecular structure and provide information on the interaction between components, which are essential for designing and testing theoretical models of mixtures [2]. Critical parameter is an important property required in a wide range of academic research. The critical parameters of pure compounds [3-6] and binary mixtures [7-11] have been investigated by using visualization experiment method, and which has been reviewed by Hicks and Young [12]. Visualization experiment method is considered as the most accurate method for determining critical point of fluid. However, the most of the reported researches are accomplished at

* Corresponding author. Tel.: +86-10-82314545.
E-mail address: zhang_cb@sjp.buaa.edu.cn
Foundation item: National Natural Science Foundation of China (50676005)

doi: 10.1016/S1000-9361(11)60398-1

low temperature conditions. In addition, compared with pure and binary mixtures, experimental data on critical phenomenon of multi-component mixtures especially endothermic hydrocarbon fuels are scarce. In recent years, Sun, et al. [13] measured the critical point of a typical kerosene (RP-3) using flow method; the results showed that the critical pressure and critical temperature of RP-3 are 2.39 MPa and 645.5 K respectively. Hitch and Karpuk studied the heat transfer and flow instabilities of methylcyclohexane and JP-7 fuels at supercritical conditions [14-15]. Tran and Lea-Der reported heat transfer properties of endothermic fuel Norpar-12 at supercritical conditions [16]. Some researchers also investigated deposition of hydrocarbon fuels [17-19]. In our previous works [20-22], the enthalpies of RP-3 at supercritical conditions and the densities of RP-3 at both sub- and supercritical conditions have been measured; moreover, the heat transfer phenomenon of RP-3 flowing through a U-turn tube has been studied.

In this work, the flow phenomenon including critical opalescence of RP-3 has been experimentally investigated using visual experiment technique at both high temperature and pressure conditions. The paper is organized as follows: in Section 2, the experimental apparatus and procedures are described; in Section 3, the flow phenomenon at different inlet temperatures and pressures are exhibited and the effects of pressure, temperature and flow orientation to the flow phenomenon are analyzed; in Section 4, we end this study with concluding remarks.

2. Experimental Apparatus and Procedures

2.1. Materials

A typical jet fuel RP-3 is used in this work. Composition analysis by using GC6890-MS5975 shows that RP-3 consists of 52.44% alkanes, 7.64% alkenes, 18.53% benzenes, 15.54% cycloalkanes, 4.39% naphthalenes and 1.46% others; the detailed compositions of RP-3 are listed in Table 1.

In addition, the initial boiling point (IBP) and the final boiling point (FBP) of RP-3 at 0.1 MPa are identified by using ASTM D2887 and corrected by ASTM-D86 correlation, which are 390.8 K and 530.1 K, respectively.

2.2. Facility

Figure 1 shows the experimental system. It includes preparative system, measured system and reclaimed system.

In the preparative system, the fuel in Tank 1 is pumped up to 12 MPa by a piston pump (2J-Z 104/16). A 45 micron filter (Filter 1) is attached to the suction side of the pump to protect the pump from any entrained debris and serve as an inlet accumulator to ensure the pump is not starved on the suction stroke. The pre-pressurized fuel from the piston pump is pushed into an attached airbag pulsation damper (NXQ-L04/16-H) so that the pressure pulsation could be reduced to lower than 0.5% of the test section inlet pressure. The fuel from the damper is divided into a major path fuel and a bypass fuel: the latter is collected for reuse and its pressure is controlled by a back pressure valve 0-15 MPa in the bypass system; the mass flow rate of the major path fuel is measured using a Corio-

Table 1 Detailed analysis of fuel composition for RP-3 jet fuel

No.	Composition	Mass fraction/%
1	*n*-hexane	0.37
2	*n*-octane	0.76
3	*n*-nonane	2.52
4	*n*-decane	5.78
5	*n*-undecane	4.39
6	*n*-dodecane	3.84
7	*n*-tridecane	3.21
8	*n*-tetradecane	1.65
9	*n*-pentadecane	0.57
10	*n*-hexadecane	0.59
11	*n*-heptadecane	3.08
12	2-methyloctane	1.08
13	3-methyloctane	1.53
14	4-methyloctane	1.72
15	2-methylnonane	0.93
16	3-methylnonane	1.05
17	4-methylnonane	1.28
18	2-methyldecane	1.45
19	3-methyldecane	1.55
20	4-methyldecane	1.78
21	5-methyldecane	1.94
22	2-methylundecane	1.48
23	3-methylundecane	1.66
24	4-methylundecane	1.70
25	5-methylundecane	2.25
26	2-methyldodecane	0.76
27	3-methyldodecane	0.93
28	4-methyldodecane	1.28
29	5-methyldodecane	1.33
30	6-dimethyl-2-octene	1.87
31	4-propyl-3-heptene	3.18
32	2-methylpentalene	2.59
33	1,2,3-trimethyl-benzene	4.48
34	1,3,5-trimethyl-benzene	3.27
35	1-ethyl-3-methyl-benzene	7.81
36	2-ethenyl-1,3-dimethyl-benzene	2.98
37	Cyclododecane	1.17
38	1-hexylcyclopentane	4.20
39	1-butyl-2-ethyl-cyclopentane	1.34
40	1,1,3-trimethyl-cyclohexane	2.11
41	1-butylcyclohexane	4.28
42	1-heptylcyclohexane	0.56
43	1-ethyl-4-methylcyclohexane	1.87
44	1-methyl-naphthalene	2.45
45	2-methyl-naphthalene	1.94
46	Other	1.46

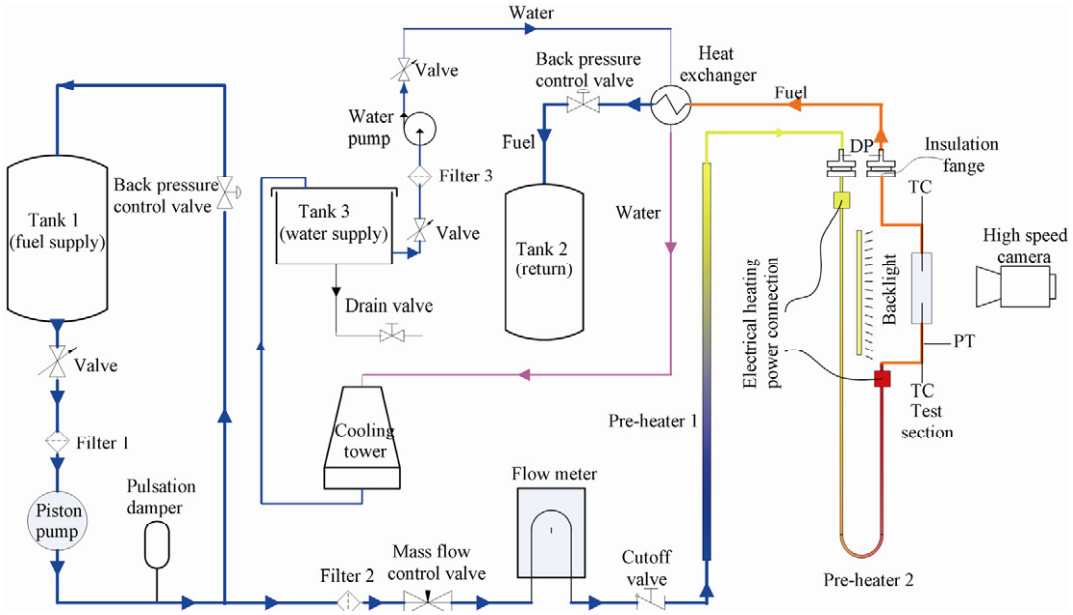

Fig. 1 Schematic of experimental system.

lis-force flow meter (DMF-1-1, 0.15%) and a 30 micron filter is installed to the upstream of the flow control valve (SS-426F3) to protect the fine passages in it. In order to achieve the required inlet fuel temperature of the test section, the pre-pressurized major path fuel is heated (up to 830 K) by two pre-heaters (Pre-heater 1 and Pre-heater 2) which are controlled by independent available current power supplies with a capacity of 20 kW. In the test section, a pressure gauge transducer (3051CA4A, Rosemount) is used to measure the static pressure at the inlet of the test section, and the fuel pressure of the test section is controlled by a back pressure valve 0-15 MPa. The fuel temperature is measured at the inlet and exit with K-type armored thermocouples respectively. When experiments run, the backlight is turned on, and the flow pattern in test section is captured by high speed camera (IDT XStream Vision XS-3) with 400 flames per second. All data are recorded using computer system.

After testing, the hot fuel is cooled lower than 310 K by a water cooled shell and tube heat exchanger. At last the fuel pressure decreases to ambient pressure through a back pressure valve 0-15 MPa in the major path and is collected into Tank 2 for other usages. The water out of heat exchanger is cooled in cooling tower and then collected into Tank 3 for recycling.

2.3. Test hardware

The detailed configuration of the test section is illustrated in Fig. 2. The inside and outside diameters, and the length of the quartz-glass tube are 6 mm, 20 mm, and 100 mm respectively. Two expanded graphite gaskets are installed between stainless steel sealed plate and quartz-glass tube to ensure there is no leakage of fuel when temperature is lower than 830 K at 5 MPa pressure condition. The covers are connected with bearing cylinder through thread. A glass window (15 mm × 40 mm) is attached to the side of bearing cylinder to permit full visibility of the flow patterns. A four-way and a T-type connection are connected to each side of sealed plate for the connections of K-type thermocouple and pressure transducer. And the test section is isolated with aspen (an insulating compound) except for the part of the view window.

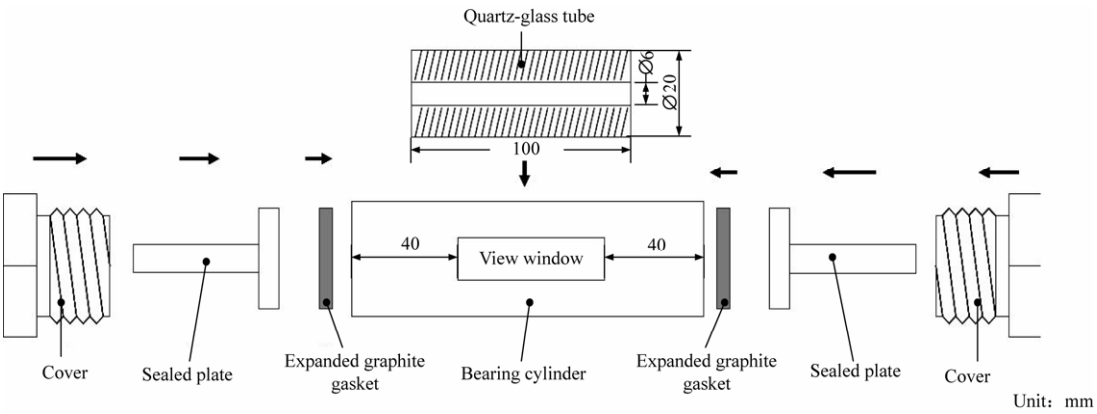

Fig. 2 Schematic of test section.

2.4. Rig calibration

Calibration of the mass flow meter through the data acquisition system is accomplished by weighing several fluids over timed intervals at a constant upstream pressure and flow rate through a metering valve, and the accuracy is ±0.15% of the reading value. The pressure gauge transducer is calibrated with the pressure calibrator (Mensor PCS400M), and the maximum uncertainty is ±0.065% of the full range of 10 MPa. All the thermocouples are calibrated in a constant temperature bath and the measurement accuracy is found to be ±0.2 K.

3. Results and Analysis

3.1. Flow patterns of RP-3

In this work, visualization experiments of fuel flow patterns are carried out in vertical quartz-glass tube with the inner diameter of 6 mm. In the experiments, the mass flow rate is fixed at g = 30 g/min, corresponding to the Reynolds number from 100 at 300 K to about 4 000 at 750 K.

Cheng, et al. [23] gives a good review of two-phase flow patterns and Fig. 3 shows the most commonly observed adiabatic two-phase flow patterns in vertical tube, which includes bubble flow, slug flow, churn flow, annular flow, wispy-annular flow and mist flow. All of which have been observed in our experiments. In the following text, the details of these flow patterns will be described.

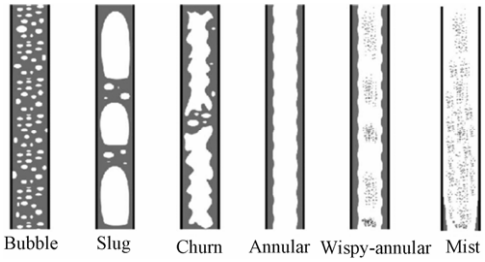

Fig. 3 Schematic of flow patterns in vertical upward gas-liquid cocurrent flow [23].

3.1.1. Effect of temperature on flow pattern

Figure 4 shows the flow patterns of RP-3 at different inlet temperatures. The inlet pressure is fixed at the pressure p = 0.107 MPa; the blue arrow indicates flow direction, which is vertical upward flow; the temperature T is the inlet temperature. The flow patterns are recorded from the glass window using high speed camera with the frequency of 400 Hz. In the experiments, flow pattern transitions are induced by increasing inlet temperature of the test section because the boiling temperature of RP-3 at atmosphere pressure is not a fixed temperature but a region because RP-3 is multi-component mixture. It can be seen that a relative

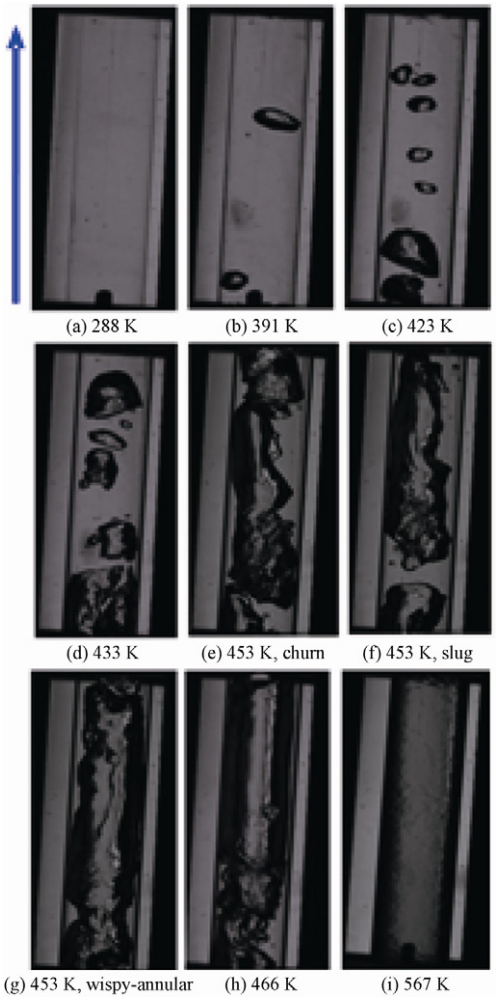

Fig. 4 Flow patterns of RP-3 under different inlet temperature (p=0.107 MPa, g = 30 g/min).

small quantity of kerosene vapor is generated when fluid temperature reaches IBP (390.8 K). When the temperature increases to 423 K, bubble flow is formed (see Fig. 4(c)). When the main stream temperature reaches 433 K, the rate of kerosene vapor generation increases and lots of small bubbles congregate. Then slug flow (see Fig. 4(d)), which consists of a regular train of large bubbles separated by liquid slugs, is observed. Each of these bubbles occupies nearly the entire channel cross section except for a thin liquid layer on the wall, and their length is typically one to two times of the channel diameter [23]. As the temperature increases to 453 K, the quantity of kerosene vapor increases to a relatively higher value. The larger bubbles combine and firstly induce an unstable flow pattern of churn flow (see Fig. 4(e)). At the same time, intermittent slug flow (see Fig. 4(f)) and wispy-annular flow (see Fig. 4(g)) patterns are both observed. After this, the quantity of vapor continues to increase and form vapor core in the centre of tube. Most of the liquid is pushed to the wall; only small quantities of liquid droplets congregate to form bunchy liquid and then wispy-annular flow is formed (see Fig. 4(g)). Very high temperature (466 K) can cause higher kerosene vapor

flow rate and then generates annular flow (see Fig. 4(h)). At even higher temperature, all the liquid is sheared from the wall to form the mist flow (see Fig. 4(i)). It is deduced that the flow pattern transforms into single phase vapor flow when the temperature increases continually. The results show that the inlet temperature can change the flow pattern independently. The bubble is generated with the increase of inlet temperature; the higher the temperature, the more the kerosene vapor quatity, and then the flow transforms from single liquid flow to mist flow.

3.1.2. Effect of pressure on phase transition

Figures 4-5 show the phase transition of RP-3 at sub-critical pressure. In the experiments, the temperature changes from room temperature to 611.4 K under pressures from 0.107 MPa to 2.07 MPa; the mass flow rate is fixed at 30 g/min. It can be seen that when the inlet pressure is 0.107 MPa, the bubble generates at the temperature of T = 391 K; when the pressures are increased to 1 MPa and 2.07 MPa, the temperatures of bubble generation increase to T = 528 K and T= 601.3 K, respectively. Similar to most fluids [24], the temperature of bubble generation increases with the increase of pressure. Under the sub-critical pressure condition, the relationship of pressure and boiling temperature is described as

$$\lg p = A + B/T \tag{1}$$

where A and B are coefficients, which are constants.

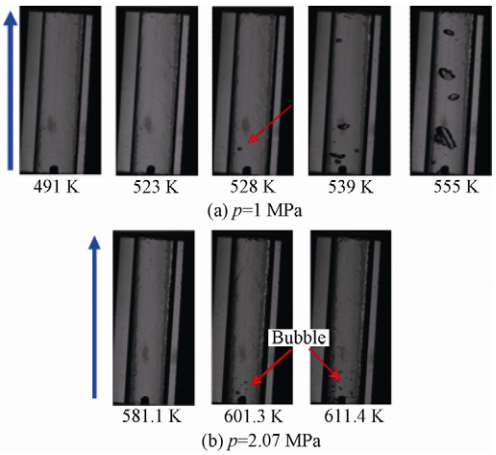

Fig. 5 Transition processes of flow pattern at sub-critical pressure (upward flow).

According to the data of boiling temperatures of RP-3, A and B are identified as 2.789 369 and −1 480.225, respectively. Thus

$$\lg p = 2.789\,369 - 1\,480.225/T \tag{2}$$

The results reveal that the flow pattern transforms more difficultly for higher inlet pressure. In addition, the pictures also indicate that at the same mass flow rate, the size of bubble decreases and the shape of the bubble is more flat with the increase of inlet pressure. The shape of phase interface is described by Young-Laplace equation [25]:

$$\Delta p = \gamma_{12}\left(\frac{1}{R_1}+\frac{1}{R_2}\right)+C_{\mathrm{H}}\frac{1}{R_1R_2} \tag{3}$$

where γ_{12} stands for the interfacial tension, Δp for the difference of pressure along the interface, C_{H} for the bending stress and R_1 and R_2 for the principal radii of curvature. Curvature measures the local bending of a curve or surface.

According to Eq. (3), the difference of pressures along the phase interface is dependent on the interfacial tension, the bending stress and principal radii of curvature. The surface tension of RP-3 decreases with the increase of pressure and temperature. At a fixed temperature, the interfacial tension decreases with the increase of pressure which leads to the shape of bubble changes to be flat. This phenomenon indicates that the curvature radii increase with the increase of pressure and temperature. The higher the system pressure, the less the surface tension and pressure difference. In addition, the flat shape is more easily fragmented to small size bubbles. It can be inferred that no bubble forms in the fluid when pressure reaches to a certain value which is named as critical pressure. Near the critical point, fluid properties exhibit liquid-like densities, gas-like diffusivities and pressure-dependent solubility. Surface tension and enthalpy of vaporization approach zero, and the isothermal compressibility and specific heat increase significantly [26]. When the pressure and temperature both increase to the critical point, the surface tension and bending stress of RP-3 are zero, thus the difference of pressure along the interface is also zero which confirms the inference above.

3.2. Critical opalescence

At the critical point, a special phenomenon called critical opalescence occurs. Critical opalescence is an optical refraction and scattering phenomenon due to large density fluctuation [10].

Figure 6 shows the influence of temperature on the process of the occurrence of the critical opalescence in upward flow. In the experiments, the inlet pressure and mass flow rate are maintained at 2.35 MPa and 30 g/min respectively. Figure 6 firstly shows that no bubble but critical opalescence occurs between 643.16 K and 648.61 K, which indicates that the critical temperature of RP-3 is in this range. As inlet temperature increases, the phenomenon of critical opalescence region moves down. At last, the opalescence disappears.

The mechanism of critical opalescence is first described by Reyleigh, and the intensity of scattered light is defined as follows [27]:

$$I = \frac{2\pi^2V^2}{\lambda^4}\cdot\left(\frac{n-n_0}{n}\right)^2 = \frac{2\pi^2V^2}{\lambda^4}\cdot\left(\frac{\Delta n}{n}\right)^2 \tag{4}$$

where λ is the wavelength of light in the medium; V stands for the volume of molecules; n and n_0 rep-

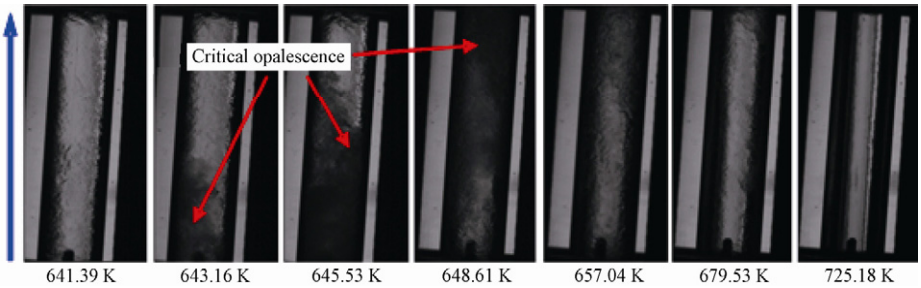

Fig. 6 Processes of critical opalescence occurrence (p=2.35 MPa, upward flow).

resent the refractive index of the molecules and the medium respectively, $\Delta n = n - n_0$.

According to the law of refraction,

$$\frac{1}{\rho}\cdot\frac{n^2-1}{n^2+2}=\text{constant} \tag{5}$$

Where ρ is the density of medium, and then the total differential of Eq. (5) is

$$\mathrm{D}\left(\frac{1}{\rho}\cdot\frac{n^2-1}{n^2+2}\right)=-\frac{\partial\rho}{\rho^2}\cdot\frac{n^2-1}{n^2+2}+\frac{1}{\rho}\cdot\frac{6n\partial n}{(n^2+2)^2}=0 \tag{6}$$

where D is the total differential symbol, thus

$$\frac{\partial n}{n}=-\frac{\partial\rho}{\rho}\cdot\frac{(n^2-1)(n^2+2)}{6n^2} \tag{7}$$

So Eq. (4) can be transformed as

$$I=\frac{2\pi^2V^2}{\lambda^4}\cdot\left[\frac{(n^2-1)(n^2+2)}{6n^2}\right]^2\cdot\left(\frac{\partial\rho}{\rho}\right)^2 \tag{8}$$

Hence, the average intensity of scattered light is

$$\overline{I}=\frac{2\pi^2V^2}{\lambda^4}\cdot\left[\frac{(n^2-1)(n^2+2)}{6n^2}\right]^2\cdot\overline{\left(\frac{\partial\rho}{\rho}\right)^2} \tag{9}$$

Due to $\frac{\partial\rho}{\rho}=-\frac{\partial V}{V}$, and according to fluctuation theory [27]:

$$\overline{\left(\frac{\partial V}{V}\right)^2}=\frac{kT}{V}\kappa_T \tag{10}$$

where k is the specific heat ratio; $\kappa_T=-\frac{1}{V}\cdot\left(\frac{\partial V}{\partial p}\right)_T$, which represents isothermal compressibility. Therefore

$$\overline{I}=\frac{2\pi^2}{\lambda^4}\cdot\left[\frac{(n^2-1)(n^2+2)}{6n^2}\right]^2\cdot\frac{kT}{V}\kappa_T \tag{11}$$

$\left(\frac{\partial p}{\partial V}\right)_T$ can be expanded through Taylor series at critical point

$$\left(\frac{\partial p}{\partial V}\right)_T=\left(\frac{\partial p}{\partial V}\right)_c+\left(\frac{\partial^2 p}{\partial V^2}\right)_c(V-V_c)+\left(\frac{\partial^2 p}{\partial V\partial T}\right)_c(T-T_c)+\cdots \tag{12}$$

where the subscript "c" stands for critical point.

At critical point,

$$\left(\frac{\partial p}{\partial V}\right)_c=0 \quad\text{and}\quad \left(\frac{\partial^2 p}{\partial V^2}\right)_c=0$$

so $\kappa_T\propto\frac{1}{T-T_c}$.

Thus, Eq. (11) can be simplified as

$$\overline{I}\propto\frac{1}{T-T_c} \tag{13}$$

Equation (13) indicates that intense light scattering phenomenon will occur when the fluid temperature gets extremely close to its critical point, which will lead the transparent fluid to transform into opaque fluid, which is called critical opalescence.

Figure 7 shows the influence of pressure on the occurrence of critical opalescence in upward flow. In the experiments, the pressure changes from 0.8 MPa to 4.99 MPa and the mass flow is 30 g/min. The results indicate that the pressure of critical opalescence occurrence also constitutes a region: the critical pressure of RP-3 is between 2.309 MPa and 2.366 MPa. According to Eq. (13), the point of the most obvious critical opalescence occurrence should be the critical point of the medium. It is shown in Fig. 7 that the most obvious critical opalescence phenomenon appears at case Fig. 7 (b) to Fig. 7(d), but only case Fig. 7(c) and Fig. 7(d) are used to identify the critical point of RP-3 because the thermocouples are completely immerged into the region filled by critical opalescence while the temperature of case Fig. 7(b) is inaccurate enough.

Thus, the critical point of RP-3 is further determined as follows: the critical temperature is between 644.55 K and 645.53 K and the critical pressure is between 2.309 MPa to 2.35MPa. In order to analyze the experimental data of heat transfer and flow phenomenon conveniently, the critical point of RP-3 is identified as (T_c = 645.04 K, p_c = 2.33 MPa), which is the average value of the pressures of 2.309, 2.33 and 2.35 MPa and the temperatures of 644.55, 645.53 K.

This result has a little difference with the result from Sun, et al. [13], which is p_c = 2.39 MPa and T_c = 645.50 K. In addition, Figs. 6-7 also show that the

fluid can be considered as a single phase flow when the fluid pressure exceeds its critical pressure because no phase change is observed under these conditions.

Figure 8 shows the effect of flow orientation on critical opalescence. The pressure and mass flow rate are 2.35 MPa and 30 g/min respectively and the inlet temperature is 645 K. The picture shows that in upward flow, the critical opalescence fills in the main part of the tube, while it is restricted in a narrow space in downward flow.

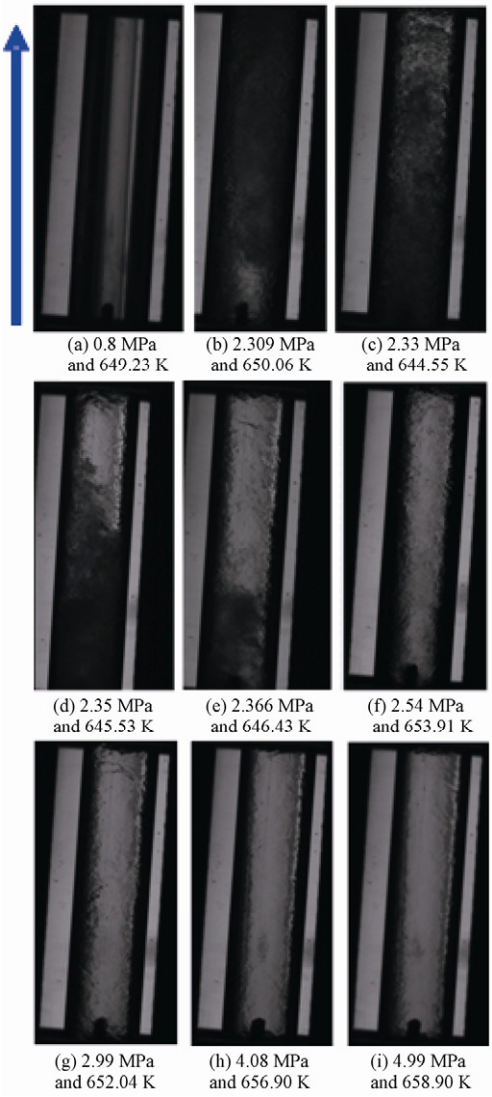

Fig. 7 Influence of pressure on critical opalescence (upward flow).

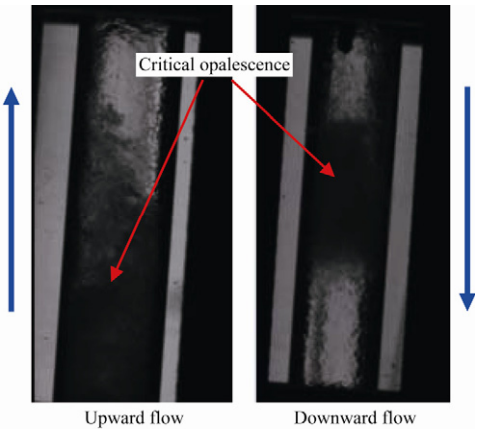

Fig. 8 Critical opalescence in upward flow and downward flow.

The results indicate that the critical opalescence is affected by the fluid inertia. This is because of the interaction of the buoyancy effect and fluid inertia. As aforementioned, critical opalescence is caused by large density fluctuation, while variable-inertia and buoyancy are two important effects caused by density variation under different conditions [28]. Usually, the significant variable-inertia effect occurs in strongly heated internal gas flow [29]. Our study is operated in adiabatic test section so that the variable-inertia effect is not significant. Thus, buoyancy effect is the main factor to affect the differences of critical opalescence for different fluid inertia. In the upward flow, the buoyancy force has the same direction as the fluid inertia, so that the microelement of the fluid which reaches the critical state previously can diffuse into the mainstream freely and the fluid inertia will enhance the process of diffusion, which causes that the most part of the quartz-glass tube is filled by critical opalescence. In the downward flow, the buoyancy force is opposite to the fluid inertia, which causes the fluid inertia to prevent the fluid microelement which reaches to critical state previously to diffuse into the mainstream.

3.3. Layered flow phenomenon in horizontal flow

Figure 9 shows effect of temperature on layered flow phenomenon in horizontal flow. In the experiments, the inlet pressure and mass flow rate are maintained at 2.38 MPa and 30 g/min respectively. The place of the interface is marked with red arrows in the figure. As aforementioned, under critical and supercritical pressure conditions, the flow state of fluid can be considered as single phase flow, thus the layered interface in Fig. 9 is not gas-liquid interface but density interface. This phenomenon only appears when the average inlet section temperature of RP-3 reaches or exceeds its critical temperature. It is the density difference between the upper flow and the bottom flow causes this phenomenon. In Fig. 9(a), the measuring point of the inlet thermocouple is immerged into the bottom fluid and the temperature is 629.57 K; this value is lower than the critical temperature of RP-3. It can be inferred that the upper fluid temperature has exceeded the critical point at that time. In order to prove this, the heating power is increased so that the interface moves down and then the inlet thermocouple can immerse into the upper fluid, as shown in Fig. 9(b) and Fig. 9(c), and the temperatures are 657.35 K and 688.35 K, respectively. The result confirms that the temperature of the upper fluid is higher than its critical point. In fact, the interface in Fig. 9(b) and Fig. 9(c) is also formed by light scattering. Under the experimental conditions, the fluid above the interface reaches super-

critical state but that below the interface has not reached the supercritical state but supercritical liquid state. Thus, the density of the upper fluid is lower than that of the bottom fluid. Moreover, it can be seen from Fig. 9 that the quantity of the bottom fluid increases along flow orientation. This phenomenon is caused by heat loss in test section: the fluid at supercritical state is cooled due to heat loss and then the fluid transforms into supercritical liquid state, which leads to the increase of the bottom fluid.

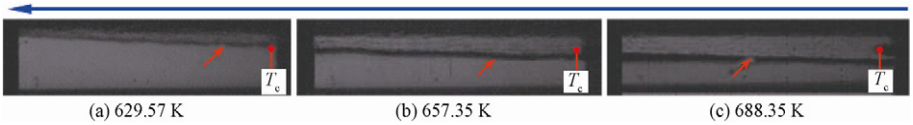

Fig. 9 Effect of temperature on layered flow phenomenon (TC-thermocouple).

Figure 10 shows the effect of pressure on layered flow phenomenon in horizontal quartz-glass tube. The pressure changes from 0.109 to 3.00 MPa and the mass flow rate is 30 g/min. The place of interface is arrowed on the figure (red arrow), and the inside surface of quartz-glass tube is marked with green bold line. As aforementioned, at ambient pressure, lots of bubbles are generated when the temperature reaches 423 K, and annular flow is formed when temperature reaches 466 K in upward flow. For horizontal flow, the obvious characteristics of annular flow pattern are that: the thickness of the bottom liquid film is much greater than that of the top liquid film due to gravity effect, and the shape of interface is undulate [23]. These characteristics can be seen from Fig. 10(a).

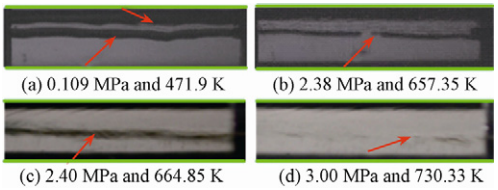

Fig. 10 Effect of pressure on layered flow phenomenon in horizontal flow.

As the pressure and temperature increase and exceed its critical point, it is also found from Fig. 10(b) to Fig. 10(d) that the interface still exists but not apparent compares with that of Fig. 10(a). In supercritical state, the interface is actually the pseudo-critical region of RP-3 for a given pressure because the properties of RP-3 at pseudo-critical point also exhibit rapid variations with a change of temperature. As mentioned above, the interface is observed through optical refraction and scattering phenomenon which is caused by density difference. At supercritical pressure, density differences decrease with the increase of pressure, which leads to the fact that the interface is not clear at higher pressure. In addition, it can be seen from Fig. 10 that the inside wall of quartz-glass tube in Figs. 10(b)-10(d) is not transparent such as in Fig. 10(a) due to coking deposition effect at high temperatures.

4. Conclusions

1) The flow patterns of two-phase flow for RP-3 at ambient pressure are classified into six types: bubble flow, slug flow, churn flow, wispy-annular flow, annular flow and mist flow. The flow pattern can be transformed by changing fluid temperature or pressure independently.

2) Before critical point, the relationship of pressure and the boiling temperature of RP-3 is identified.

3) Under constant inlet pressure, the transient of flow pattern is more difficult as the increase of inlet temperature. For a fixed mass flow rate, the bubble size decreases with the increase of pressure and the bubble is more flat at higher subcritical pressure.

4) The critical point of RP-3 is identified as (T_c = 645.04 K, p_c = 2.33 MPa) and it is found that when the fluid pressure exceeds 2.33 MPa the flow can be considered as a single phase flow.

5) The critical opalescence phenomenon of RP-3 is observed when the temperature is within 643.16 K to 648.61 K and the pressure is between 2.308 MPa and 2.366 MPa.

6) The region filled by the critical opalescence in upward flow is clearly larger than that in downward flow due to the interaction between buoyancy force and fluid inertia. In upward flow, the critical opalescence fills the most part of the tube because the buoyancy force is with the same direction of fluid inertia; in downward flow, the direction of buoyancy force and fluid inertia is opposite, which causes the fact that the region filled by critical opalescence is restricted in a narrow space.

7) In horizontal flow, layered flow phenomenon is observed under supercritical pressure conditions due to gravity and density difference. This phenomenon only occurs when the mean inlet temperature exceeds its pseudo-critical temperature. The higher the pressure and temperature, the less the density differences and therefore the interface is not clear.

References

[1] Huang H, Spadaccini L J, Sobel D R. Fuel-cooled thermal management for advanced aeroengines. Journal of Engineering for Gas Turbines and Power 2004; 126(2): 284-293.

[2] Lei Y, Chen Z, An X, et al. Measurements of density and heat capacity for binary mixtures {x benzonitrile + (1−x) (octane or nonane)}. Journal of Chemical & Engineering Data 2010; 55(10): 4154-4161.

[3] Fujiwara K, Nakamura S, Noguchi M. Critical parameters and vapor pressure measurements for

1,1,1-Trifluoroethane (R-143a). Journal of Chemical Engineering 1998; 43(1): 55-59.
[4] Rosenthal D J, Gude M T, Teja A S, et al. The critical properties of alkanoic acids using a low residence time flow method. Fluid Phase Equilibria 1997; 135(1): 89-95.
[5] Nikitin E D, Pavlov P A, Skipov P V. Measurement of the critical properties of thermally unstable substances and mixtures by the pulse-heating method. The Journal of Chemical Thermodynamics 1993; 25(7): 869-880.
[6] Smith R L, Jr, Teja A S, Kay W B. Measurement of critical temperatures of thermally unstable *n*-Alkanes. AIChE Journal 1987; 33(2): 232-238.
[7] Kordikowski A, Robertson D G, Poliakoff M. Acoustic determination of the helium content of carbon dioxide from He head pressure cylinders and FT-IR studies of the density of the resulting supercritical CO_2: implications for reproducibility in supercritical experiments. Analysis Chemistry 1996; 68(24): 4436-4440.
[8] Kordikowski A, Robertson D G, Aguiar-Ricardo A I, et al. Probing vapor: liquid equilibria of near-critical binary gas mixtures by acoustic measurements. The Journal of Physical Chemistry 1996; 100(22): 9522-9526.
[9] Debye P, Caulfield D, Bashaw J. Critical opalescence of binary mixtures: perfluorotributylamine isopentane. The Journal of Chemical Physics 1964; 41(10): 3051-3054.
[10] Chu B. Critical opalescence of a binary liquid mixture, *n*-Decane—beta, beta [prime]-dichloroethyl ether. I. light scattering. The Journal of Chemical Physics 1964; 41(1): 226-234.
[11] Heng-Joo N, Robinson D B. Equilibrium-phase properties of the toluene-carbon dioxide system. Journal of Chemical & Engineering Data 1978; 23(4): 325-327.
[12] Hicks C P, Young C L. Gas-liquid critical properties of binary mixtures. Chemical Reviews 1975; 75(2): 119-175.
[13] Sun Q M, Mi Z T, Zhang X. Determination of critical properties (T_c , p_c) of endothermic hydrocarbon fuels RP-3 and simulated JP-7. Journal of Fuel Chemistry and Technology 2006; 34(4): 466-470. [in Chinese]
[14] Hitch B, Karpuk M. Experimental investigation of heat transfer and flow instabilities in supercritical fuels. AIAA-1997-3043, 1997.
[15] Hitch B, Karpuk M. Enhancement of heat transfer and elimination of flow oscillations in supercritical fuels. AIAA-1998-3759, 1998.
[16] Tran L B, Lea-Der C. Heat transfer of calculation of an endothermic fuel at supercritical conditions. AIAA-1998-3762, 1998.
[17] Wickham D T, Engel J R, Rooney S, et al. Additives to improve fuel heat sink capacity in air/fuel heat exchangers. Journal of Propulsion Power 2008; 24(1): 55-63.
[18] Edwards T, Zabarnick S. Supercritical fuel deposition mechanisms. Industrial Engineering Chemistry Research 1993; 32(12): 3117-3122.
[19] Marteney P J, Spadaccini L J. Thermal decomposition of aircraft fuel. Journal of Engineering for Gas Turbines and Power 1986; 108(4): 648-653.
[20] Zhang C B, Tao Z, Xu G Q, et al. Heat transfer investigation of the sub- and supercritical fuel flow through a U-turn tube. Turbine-09, the ICHMT Int Symposium on Heat Transfer in Gas Turbine Systems. 2009.
[21] Zhang C B, Deng H W, Xu G Q, et al. Enthalpy measurement and heat transfer investigation of RP-3 kerosene at supercritical pressure. Journal of Aerospace Power 2010; 25(2): 331-335. [in Chinese]
[22] Deng H W, Zhang C B, Xu G Q, et al. Density measurements of endothermic hydrocarbon fuel at sub- and supercritical conditions. Journal of Chemical & Engineering Data 2011; 56(6): 2980-2986.
[23] Cheng L X, Ribatski G C, Thome J R. Two-phase flow patterns and flow-pattern maps: fundamentals and applications. Applied Mechanics Reviews 2008; 61(5): 050802-050826.
[24] Lemmon E W, McLinden M O, Huber M L. NIST reference fluid thermodynamic and transport properties-REFPROP, version 7.1. National Institute of Standards and Technology, 2003.
[25] Rodríguez-Valverde M A, Cabrerizo-Vilchez M A, Hidalgo-Alvarez R. The Young-Laplace equation links capillarity with geometrical optics. European Journal of Physics 2003; 24(2): 159-168.
[26] Yang V. Modeling of supercritical vaporization, mixing, and combustion processes in liquid-fueled propulsion systems. Proceedings of the Combustion Institute 2000; 28(1): 925-942.
[27] Li H Y. Fluctuation theory. Cheng C W, Dong Q J, Peng S R, et al. Thermodynamics and statistical physics. Kaifeng: Henan University Press, 1987; 317-325. [in Chinese]
[28] Bae J H, Yoo J Y, Choi H, et al. Effects of large density variation on strongly heated internal air flows. Physics of Fluids 2006; 18(7): 075102-075126.
[29] Shehata A M, McEligot D M. Mean structure in the viscous layer of strongly-heated internal gas flows. Measurements. International Journal of Heat and Mass Transfer 1998; 41(24): 4297-4313.

Biographies:

DENG Hongwu is an associate professor of Beihang University. His main research interests are heat and transfer in aero-engines.
E-mail: denghw@buaa.edu.cn

ZHANG Chunben is a Ph.D. of Beihang University and an engineer of Xi'an Aerospace Propulsion Institute. His main research interests are flow and heat transfer in aero-engines and rocket engines.
E-mail: zhang_cb@sjp.buaa.edu.cn

TAO Zhi is a professor of Beihang University. His main research interests are heat and mass transfer in aero-engines.
E-mail: tao_zhi@buaa.edu.cn